JOURNAL OF APPLIED PHYSICS **104**, 014308 (2008)

Electrical analysis of individual ZnO nanowires

K. Subannajui,[1,a)] D. S. Kim,[2] and M. Zacharias[1,2]
[1]*IMTEK, Faculty of Applied Science, Albert-Ludwigs-University Freiburg, Georges-Köhler-Allee, 79110 Freiburg, Germany*
[2]*Max Planck Institute of Microstructure Physics, Weinberg 2, 06120 Halle, Germany*

(Received 18 February 2008; accepted 6 May 2008; published online 10 July 2008)

We report the electrical properties of individual as-grown ZnO nanowires (NWs) on SiO_2/Si and GaN/sapphire substrates. Carrier transport in metal-semiconductor-metal junction is interpreted in terms of thermionic emission and tunneling current which was assumed to dominate independently on reverse and forward contacts. Current flow in ZnO NWs grown on SiO_2/Si was dominated by thermionic emission. In contrast, both thermionic emission and tunneling current contributed to the transport in ZnO NWs epitaxially grown on GaN/sapphire. Carrier concentrations of ZnO NWs were estimated to be around 8.88×10^{17} cm^{-3} if grown on SiO_2/Si and 1.18×10^{18} cm^{-3} if grown on GaN/sapphire, respectively. © *2008 American Institute of Physics*. [DOI: 10.1063/1.2953172]

I. INTRODUCTION

Semiconducting nanowires (NWs) are increasingly interesting due to their potential use in advanced electronic and optoelectronic devices.[1] In particular, ZnO NW with a direct band gap of 3.4 eV and a large exciton binding energy of 60 meV is an important functional oxide material.[2] Recently, the high performance of field-effect transistor (FET) using a ZnO NW as an active channel has been demonstrated.[3] The performance of these *n*-type ZnO NW transistors matches characteristics observed for *p*-type carbon nanotube transistors. The FETs are reported to have a field-effect mobility of 928 cm^2/V s, a transconductance of 3.06 μS, and an on/off current ratio of 10^6.

Most transistor devices based on semiconducting NWs relied on the lithographic fabrication methods, which require aligning the NWs and defining contact pads on the substrate by using an electron beam or focused ion beam (FIB) lithography to reliable contact NWs electrically. However, these fabrication methods might also have an influence on the later evaluated characteristic data. Thus, the electrical transport studied in as-grown NWs is of importance for designing NWs for vertically aligned semiconducting NW devices. Hence, a characterization method is desired to estimate the electrical parameters of NWs without complicated steps and damages originated from electron or ion beam. Such damage observations was shown and discussed, for instance, by the papers of Zhan *et al.*[4] and Coleman *et al.*[5] Several studies of the electrical properties of semiconducting NWs have been performed using a conductive scanning force microscopy as a tool.[6,7] The lack of control on the contact formation and the poor mechanical contact stability, however, limited reliable investigations of transport characteristics. Recently, the electrical properties of single as-grown Si NWs were measured by probing them in a scanning electron microscope (SEM) using a nanomanipulator equipped with a metal tip.[8] This technique allows to measure reliable characterizations on individual NWs with flexible contacts. However, Schottky barriers at the metal-NW interface are inevitably formed due to the limited choices of metals that can be used for the tips in the measurements, which eventually complicates the carrier transport.

In this study, we investigated the electrical properties of individual as-grown ZnO NWs by using nanomanipulators equipped with Pt/Ir tips used to probe the ZnO NWs in the SEM. We compared the carrier transport in metal-NW-metal junctions for ZnO NWs grown on different substrate configurations. In our experiments, ZnO NWs on SiO_2/Si and GaN/sapphire substrates were grown and electrically characterized. The obtained results will be discussed in terms of thermionic emission and tunneling based on metal-semiconductor-metal (MSM) junctions (i.e., a back-to-back pair of Schottky barriers).

II. EXPERIMENTAL DETAILS

ZnO NWs were grown on SiO_2/Si (the thickness of SiO_2 is 100 nm) and GaN/sapphire substrates by physical vapor deposition method using Au colloids as catalyst. To disperse Au nanoparticles on the substrates, a diluted Au colloid solution was dropped and subsequently dried by blowing Ar gas after a few seconds. Then the samples were cleaned using an O_2 plasma at a power of 150 W for 2 min followed by annealing the sample at 500 °C for 30 min. The growth experiments were carried out in a tube furnace using ZnO and graphite as source material. Prior to growth a tube pressure of 200 mbars was maintained under a constant Ar flow of 30 SCCM (SCCM denotes cubic centimeter per minute at STP). Typical growth temperatures and times were 850–920 °C and 30–60 min, respectively. The NW samples were kept in air after growth.

The electrical characterization of ZnO NWs was carried out inside a high-resolution SEM JEOL JSM 6400, equipped with a nanomanipulator pair (Kleindiek). The manipulators are equipped with Pt/Ir tips, which are used for connecting and manipulating the NWs. The tips were electrochemically etched from 250 μm thick wires (Pt/Ir 80:20, GoodFellow) using an etching procedure described before.[9] A picoampe-

[a)]Electronic mail: kittitat.subannajui@imtek.uni-freiburg.de.

 © 2008 American Institute of Physics

Downloaded 23 Oct 2008 to 85.232.23.177. Redistribution subject to AIP license or copyright; see http://jap.aip.org/jap/copyright.jsp

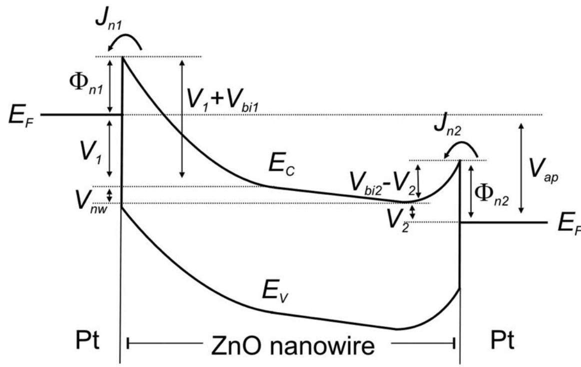

FIG. 1. Schematic diagram of MSM under an applied voltage. Positive bias is applied to the right and negative bias is applied to the left.

remeter with an internal voltage source was connected to the Pt/Ir tip for the *I-V* measurements, which were performed under computer control. For the experiment using as-grown ZnO NWs on SiO_2/Si substrate, the NW diameter was 40 nm; in the case of the as-grown ZnO NW on GaN/sapphire substrate, we used a coned NW of a diameter of 80–200 nm. The length of the wires was in the range of 3–5 μm and looks shorter in the SEM due to tilting.

A. Calculation of carrier transport in a MSM structure

1. Thermionic emission

The current flow of a metal-NW-metal structure is basically caused by the transport of charge carriers through a back-to-back pair of Schottky contact.[10] If voltage is applied at the MSM junction, one of the junctions is biased in the forward and the other in the reverse direction. The dominant carrier transport mechanisms of a MSM structure are thermionic emission over the barrier and tunneling assisted by interface states existing in the metal-semiconductor contact.

In this section, we consider only the thermionic emission as a mechanism for a carrier transport in the MSM junction. MSM analysis had been introduced by Sze *et al.*, based on thermionic theory.[10] The transport behaviors in a MSM structure can be categorized into three different regimes: (1) $V_{ap} < V_{RT}$, (2) $V_{ap} > V_{RT}$, and (3) $V_{ap} > V_{FB}$, where V_{ap} is the applied voltage, V_{RT} is the reach through voltage, and V_{FB} is the flatband voltage, respectively. The transport mode depends mainly on the depletion width, where W_{RT} is the depletion width in the fully depleted condition. When W_{RT} is equal the NW length L then V_{RT} becomes the reach through voltage. We assume in Fig. 1 that a voltage biases the left contact in reverse direction. The applied voltage is split between the two contacts; the larger voltage will drop at the reverse-biased contact. Now we put in the additional term for the boundary condition.[10]

$$V_{ap} = V_1 + V_2 + V_{NW}, \tag{1}$$

with V_{NW} the voltage drop in the NW. The last term would be negligible if the voltage drop from contacts is high. We now simplify that $V_{ap} - V_{NW} = V$ and assume that the length of NW is long enough in order to exclude a fully depleted condition (e.g., the depletion width from both ends of a NW is smaller than the length of a NW). Hence, we focus on the regime of $V_{ap} < V_{RT}$.

Majority charge carriers in ZnO NWs are electrons since ZnO normally exhibits *n*-type conductivity due to the native defects or background impurities.[11,12] Under the low voltage mode of an *n*-type semiconductor, the current is dominated by majority carriers, which would not be the case at higher applied voltage, because the ratio between electron and hole conductances can be modified. Minority carriers, holes, would be injected for several orders lower when the applied voltage is higher than reach through voltage.[10]

The reverse current and forward current are then given by

$$J_{n1} = J_{s1}\left[1 - \exp\left(-\frac{qV_1}{kT}\right)\right] \tag{2}$$

and

$$J_{n2} = J_{s2}\left[\exp\left(\frac{qV_2}{kT}\right) - 1\right], \tag{3}$$

where q is the electronic charge, k is the Boltzmann constant, T is the absolute temperature, V_1 and V_2 are the voltage drops at the reverse and forward contacts, respectively, and J_s is the saturation current. The saturation current is given by

$$J_{s1,2} = A^*_{1,2}T^2 \exp\left[-\frac{q(\phi_{n1,2} - \Delta\phi_{n1,2})}{kT}\right]. \tag{4}$$

These equations follow the thermionic and diffusion theory.[13] A^* is the effective Richardson constant, ϕ is the barrier height, and $\Delta\phi$ is the barrier lowering due to the image force. In the case of a symmetrical MSM structure and assuming that the contact area is equal at the two contacts, both interface properties are identical. If the leakage current is negligible in low applied voltage range, then the boundary condition can be applied. Due to the current continuity, the forward current equals to the reverse current, $J_{rev} = J_{forw}$ or $J_{n1} = J_{n2}$.

The relation between the applied voltage and voltage drop at the right hand side (forward) is

$$V = -\frac{kT}{q}\ln\left[2\exp\left(-\frac{qV_2}{kT}\right) - 1\right] \tag{5}$$

and the *I-V* characteristic is

$$J = J_s\left[\frac{1 - \exp(qV/kT)}{1 + \exp(qV/kT)}\right]. \tag{6}$$

Considering the transport of majority carrier from left to right following Fig. 1, the barrier is higher at reverse contact than at forward contact, or $\phi_{n1} > (V_{bi2} - V_2)$. Obviously the relations above indicate the limited current at reverse contact. However, the reverse-limited current dominates only in the limit regime of applied voltage. Breakdown at the reverse contact will occur at higher applied voltage. This effect is very close to the *Zener effect* in semiconductor junctions.

The *I-V* characteristic of thermionic emission at room temperature is shown in Fig. 2(a) for a carrier concentration of around 10^{18} cm^{-3}, a barrier height of 0.6 V, and a contact area of 10^4 nm^2. The current prior to breakdown at reverse

Downloaded 23 Oct 2008 to 85.232.23.177. Redistribution subject to AIP license or copyright; see http://jap.aip.org/jap/copyright.jsp

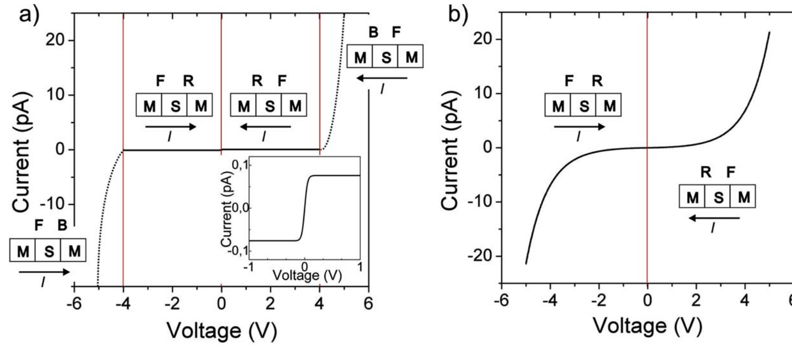

FIG. 2. (Color online) For a carrier concentration of 10^{18} cm^{-3}, a barrier height 0.6 V, a contact area of 10^4 nm^2, at room temperature. (a) *I-V* characteristic of thermionic emission. The current before breakdown at reverse contact follow Eq. (6), and the curve is very flat. The slope increases after breakdown occurs.(Note that dash lines do not come from the calculation, but the estimation of the current after breakdown.) The inset is the observation of the curve at very small current. (b) In the case of thermionic emission combined with tunneling, the curve follows Eq. (11). The slope of *I-V* is already increased without breakdown at reverse contact. The Forward (F), Reverse (R), and Breakdown (B) are labeled.

contact is following Eq. (6). The curve is very flat but there is the small steplike increase of current near 0 V, as shown in the inset of Fig. 2(a).

2. Combining thermionic emission and tunneling

We now take into account the tunneling effect, which is another major transport phenomenon observed for MSM structure. The tunneling current through the barrier in metal semiconductor was first analyzed by Padovani and Stratton in an exponential form.[14]

At reverse contact, the reverse current can be expressed by the following equation:

$$J_1 = J_{s1}\left(1 - \exp\left[-\frac{qV_1}{kT}\right]\right) + J_{t1}\exp\frac{qV_1}{E_{t1}}. \quad (7)$$

The first term is related to thermionic emission. The second term is the simplified form of the tunneling part. At room temperature, the contribution of thermionic emission at the reverse contact is negligible, but the tunneling current dominates.

At forward contact, the forward current can be expressed as follows:

$$J_2 = J_{s2}\left(\exp\left[\frac{qV_2}{kT}\right] - 1\right) + J_{t2}\exp\frac{qV_2}{E_{t2}}. \quad (8)$$

The bigger V_2 at the forward contact, the higher the contributions of thermionic emission. The additional tunneling term would cause an increase of the slop. For a long NW, where V_{ap} is always lower than V_{RT}, after $V_{ap} > V_{FB}$, the forward tunneling term disappears because the forward barrier vanished [i.e., $(V_{bi} - V_2) \rightarrow 0$].

At room temperature, the relation between V_2 and V_{ap} for the case of symmetrical MSM structure is

$$J_{t1}\exp\frac{qV}{E_{t1}}\exp\left(-\frac{qV_2}{E_{t1}}\right) = J_s\exp\left(\frac{qV_2}{kT}\right)\left[1 + \exp\frac{qV}{kT}\right] - J_s + J_{t2}\exp\left(\frac{qV_2}{E_{t2}}\right). \quad (9)$$

The *I-V* relation is

$$J = A\exp\left(\frac{qV}{kT}\right) + B\exp\left(\frac{qV}{E_{t2}}\right) - J_s, \quad (10)$$

with

$$A = J_s\left[\frac{J}{J_{t1}}\right]^{-E_{t1}/kT} \quad \text{and } B = J_{t2}\left[\frac{J}{J_{t1}}\right]^{-E_{t1}/E_{t2}}.$$

The above relation can be calculated numerically. In the case of an approximation, a very high contribution of tunneling related to reverse contact and a high contribution of thermionic emission related to forward contact is valid and the *I-V* relation becomes

$$J = A\exp(CV) + B\exp(DV) - J_s, \quad (11)$$

with

$$A = J_s\left[\frac{J_{t1}}{J_s}\right]^{E_{t2}/(kT+E_{t2})}, \quad B = J_{t2}\left[\frac{J_{t1}}{J_s}\right]^{kT/(kT+E_{t2})},$$

$$C = \frac{qE_{t2}}{E_{t1}(kT+E_{t2})}, \quad D = \frac{qkT}{E_{t1}(kT+E_{t2})}.$$

In this approximation, C should be bigger than D.

Therefore, in the combined tunneling and thermionic emission, the *I-V* curve of the MSM system should follow the double exponential function, depending on which mechanism is dominated. These equations follow the model in Fig. 1. In the case of $V < 0$, which means a change between forward and reverse J becomes $-J$, and V becomes $-V$ in the equations above.

These two exponential functions are important because they indicate the difference of the curve from ideal thermionic case. It also explains the semilinear behavior at lower voltage. If the tunneling term at forward contact is small enough then the curve becomes single exponential. In the case of $V_{ap} > V_{FB}$, one has a larger ratio of minority carrier injection and the relation of the *I-V* characteristic might be more complicated.

Figure 2(b) shows the theoretical expected *I-V* characteristic of a MSM junction when the tunneling term is taken into account in addition to the thermionic emission term. The symmetry of the curve depends on the ZnO NW properties.

Downloaded 23 Oct 2008 to 85.232.23.177. Redistribution subject to AIP license or copyright; see http://jap.aip.org/jap/copyright.jsp

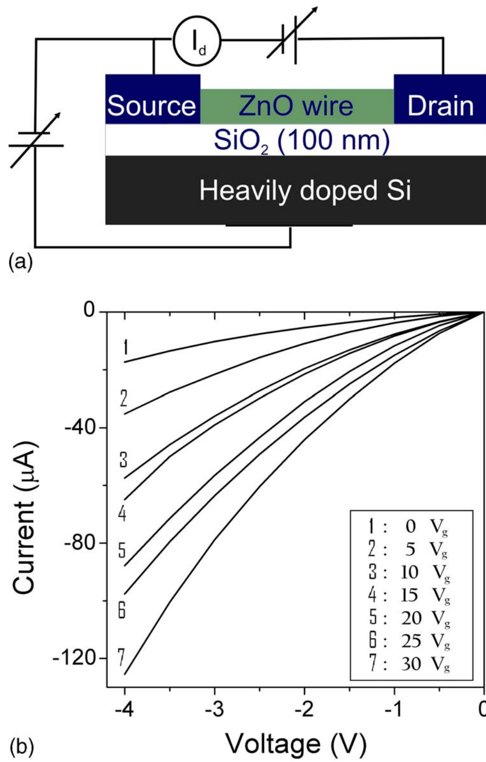

FIG. 3. (Color online) (a) Schematic of ZnO NW FET with Al/Au contact pads on the highly doped SiO_2/Si substrate. (b) The *I-V* curve for varying V_g (0–30 V, ΔV=5 V).

Hence, if carrier concentration, contact areas, and interface properties are different, the curve might not be symmetric since these properties control the effective carrier concentration at the interface and barrier characteristic. The above developed equations can now be used in MSM junction with a long conductive channel under the conditions that the NW structure is large enough to neglect a size effect (which is observed for structures below or in the range of de Broglie wavelength).

B. Conventional FET measurements

We also fabricated Ohmic contacts and FET devices based on ZnO NWs removed from the substrate to electrically compare with the as-grown ZnO NWs still on SiO_2/Si substrate. For Ohmic contacts, Al/Au contact pads using a transmission electron microscopy grid are deposited on both sides of a NW discarded flatly on a SiO_2 surface of a Si wafer. By assuming that the residual resistance at the contact pads after annealing is negligible, a linear Ohmic *I-V* curve is obtained with a resistivity in the range of 25.8 mΩ cm. For FET, with increasing positive gate voltage, the current flow is increased. Hence, it is found that, unlike in typical FETs, a FET ZnO NW collects majority carriers in the conductive channel and works in the accumulation mode.

For Fig. 3, the measurement has been done in the negative regime. However, under the assumption that the FET structure is symmetric, the interpretation on mobility and carrier concentration is consistent.

Following the mobility calculations based on the gate voltage, we expect

$$\frac{dI}{dV_g} = \mu\left[\frac{C}{L^2}\right]V_{sd}. \qquad (12)$$

The capacitance can be obtained from literature,[15]

$$C = \frac{2\pi\varepsilon_0\varepsilon_{SiO_2}L}{\ln(4h/d)}, \qquad (13)$$

where ε_{SiO_2} is the dielectric constant of the gate SiO_2, h is its thickness, and d is the wire diameter. The FET mobility is approximately 230 $cm^2/V\,s$, which is similar to the bulk value. The estimated carrier concentration was around 8.88×10^{17} cm^{-3}. The doping energy level can be calculated using

$$E_f - E_c = kT \ln\left(\frac{N_D}{N_C}\right), \qquad (14)$$

where $N_C=2(m_e^* kT/2\pi\hbar^2)^{3/2}$.

The energy difference between the Fermi level and the conduction band is 35 meV. Hence, these NWs are highly doped but not degenerated.

C. Measurements with nanomanipulator

Figure 4(a) shows a typical *I-V* characteristic of as-grown ZnO NWs on SiO_2/Si substrate. The slop of the *I-V* curve is very flat in the regime of −4 to 4 V, but the current drastically jumps above 4 V. This result is very close to the ideal thermionic emission case, which means the tunneling term is very small. We observe an unsmooth curve above 4 V. This would indicate the breakdown at reverse contact. The *I-V* curve of ZnO NWs epitaxially grown on GaN/sapphire substrate shows a quite different characteristic, as seen in Fig. 4(b). A nontrivial slop of the *I-V* curve is visible, indicating that the tunneling current along the reverse contact is higher in the case of the wires grown on GaN/sapphire substrates.

Apart from shape and size, the observed difference in *I-V* characteristic in NWs grown on the two different substrates should be interpreted in more details. In the case of the wires on GaN/sapphire substrates, one could expect an influence of a diffusion of dopant or defects originating from GaN layer, which is not the case for wires grown on SiO_2/Si substrate. It is known that photoconductivity analysis on GaN NWs shows inhomogeneous distribution of defects along the wire, an effect which is interpreted as diffusion of defects from the Si substrate during heteroepitaxial growth.[16] Even when the density of donor or defects is not achievable straightforwardly from our measurements, there is a possibility that such dopant and defect diffusion would increase the carrier concentration, which relate directly to the tunneling current.

Additionally, effects due to the surface states may also influence the *I-V* curve strongly. If there is additional oxygen or some other negative charge molecules on the surface, then band bending and state pinning would take place.[17] Then electrons require higher excitation energy, yielding a reduction of mobility and carrier concentration. In real experi-

Downloaded 23 Oct 2008 to 85.232.23.177. Redistribution subject to AIP license or copyright; see http://jap.aip.org/jap/copyright.jsp

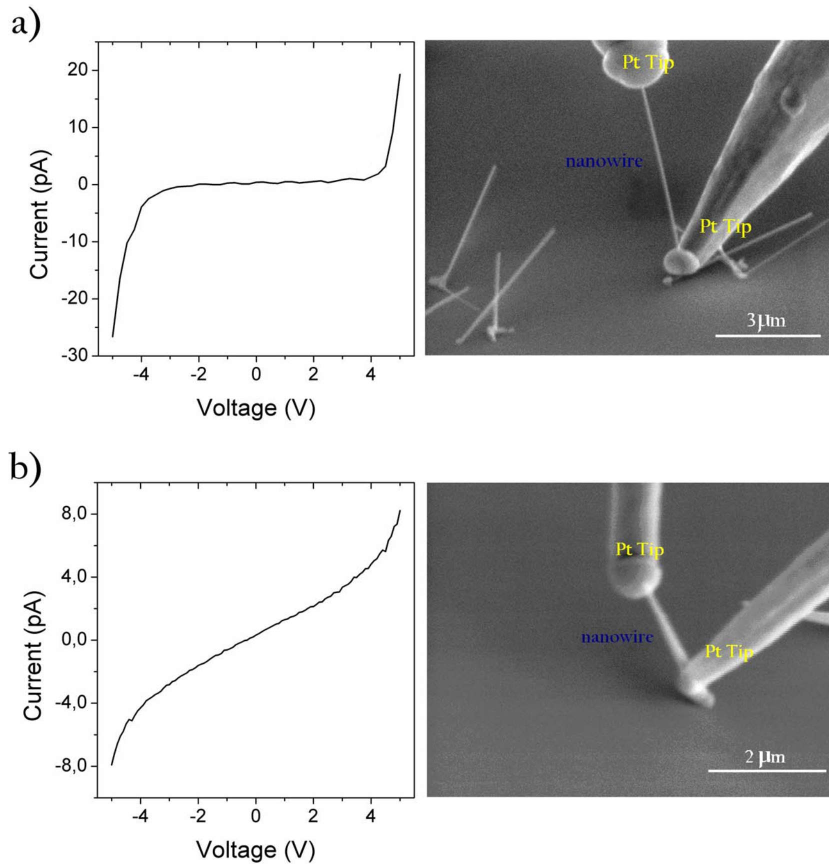

FIG. 4. (Color online) (a) *I-V* curve of as-grown ZnO NWs on SiO_2/Si substrate. Inset shows a SEM image of the ZnO NW contacted with metal tips. The NW diameter is 40 nm. (b) *I-V* curve of as-grown ZnO NW on GaN/sapphire substrate. Inset show a SEM image of the ZnO NW contacted with metal tips. The NW diameter is 80–200 nm.

ments, there is also the interaction between the applied pulse and electrostatic. The effect from the electrostatic on the barrier potential is still unknown.

In order to estimate the material property from measurement using the manipulators, the plot from the Fig. 4 is fitted with Eq. (11) under the assumption of a very high contribution of tunneling current at reverse contact and a high contribution of thermionic emission at forward contact. After fitting, the values E_{t1} and E_{t2} are obtained. E_{t1} and E_{t2} are the values from the tunneling part which is then exactly used as demonstrated in Ref. 14 (as $E_{t1}=\varepsilon'$ and $E_{t2}=E_0$). Hence, carrier concentration can be calculated.

However, if the contribution of the reverse tunneling current is too small then the carrier concentrations cannot be estimated because the curve cannot be fitted properly with Eq. (11), that is, the case in Fig. 4(a), where a breakdown occurs near ± 4 V seen by a sudden jump of the curve. Therefore, in this case, the *I-V* curve of as-grown ZnO nanowires on SiO_2/Si substrate cannot be used for the carrier concentration calculation from Eq. (11). However, by using the FET as done in Sec. II B, the carrier concentration of the as-grown ZnO NWs on SiO_2/Si was calculated. Now, for the case of the as-grown ZnO NW on GaN/sapphire substrate [Fig. 4(b)], the resulting curve fitting by a double exponential function [Eq. (11)] is demonstrated in Fig. 5 and obviously gives a good fitting. However, the resolution of our instrument is in the range of 10^{-12} A. Moreover, the fit current equal or below this value should not be safely interpreted. Hence we avoid drawing out the information of fitting from I_s. E_{t2} is around 8.43×10^{-20} J which is different from the theoretical value,[12] 4.345×10^{-21} J, by about five times, but still in the same order. For E_{t1}, the measuring value is 5.302×10^{-20} J compared to the theoretical value is 6.8×10^{-20} J. Hence, the measured value is in the same order as the theoretical value. The carrier concentration from E_{t1} is around 1.18×10^{18} cm^{-3}. Therefore, the carrier concentration of as-grown ZnO NW on GaN/sapphire substrate estimated by using the nanomanipulators is 1.18×10^{18} cm^{-3}; the carrier concentration of as-grown ZnO NW on SiO_2/Si substrate estimated by using the FET is around 8.88

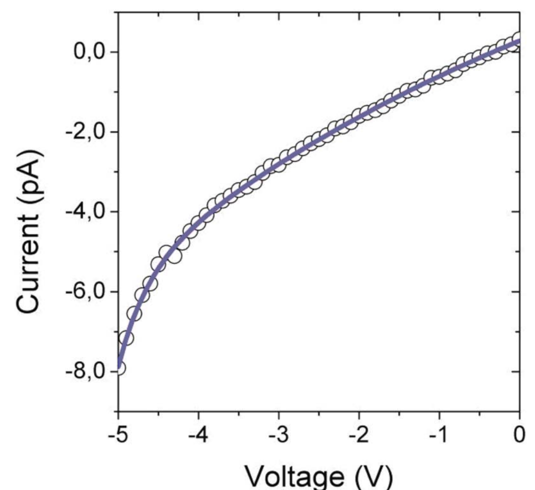

FIG. 5. (Color online) Fitting curve with double exponential function, $J = a + b\exp cV + d\exp fV$.

Downloaded 23 Oct 2008 to 85.232.23.177. Redistribution subject to AIP license or copyright; see http://jap.aip.org/jap/copyright.jsp

$\times 10^{17}$ cm^{-3}. So, one can assume that the ZnO NWs (using both kinds of substrates but the same growth condition) are highly doped but not degenerated.

III. CONCLUSION

Electrical properties of individual as-grown ZnO NWs by using nanomanipulators equipped with Pt/Ir metal tips are investigated. We applied the model of current transport in a MSM junction for the measured NWs. The results are discussed analytically in terms of thermionic emission and tunneling current from both sides of contacts. The total current is limited by reverse contact. With a higher applied voltage, the tunneling current plays a role through the reverse barrier. The opposite effect occurs at forward current. The higher the applied voltage, the higher is the contribution to the thermionic emission. By comparison between analytical calculation of MSM and experiments data of ZnO NW grown on GaN/sapphire substrate, we suggested that the current through the ZnO NWs grown on GaN/sapphire is dominated by tunneling at low voltage regime, whereas it is not the case for wires grown on SiO_2/Si substrate. Carrier concentrations of ZnO NWs on SiO_2/Si and GaN/sapphire were estimated to be around 1.18×10^{18} cm^{-3} and 8.88×10^{17} cm^{-3}, respectively. Thus, the measurements using nanomanipulators are reliable to estimate the carrier concentration and can be used as a simple and straightforward way, avoiding the more complicated FET structure and the here needed lithography.

ACKNOWLEDGMENTS

We thank J. Bauer, P. Das-Kanungo, O. Breitenstein, S. Senz, T. Shimizu, and M. Alexe for technical helps and A. Dadgar and A. Krost for supplying GaN/sapphire substrates. We also thank to P. Srivilai for a fruitful discussion of semiconductor junction theory.

[1] Y. Li, F. Qian, J. Xiang, and C. M. Lieber, Mater. Today **9**, 18 (2006).
[2] C. Klingshirn, Phys. Status Solidi B **244**, 3027 (2007).
[3] S. N. Cha, J. E. Jang, Y. Choi, G. A. J. Amaratunga, G. W. Ho, M. E. Welland, and D. G. Hasko, Appl. Phys. Lett. **89**, 263102 (2006).
[4] J. Zhan, Y. Bando, J. Hu, and D. Golberg, Appl. Phys. Lett. **89**, 243111 (2006).
[5] V. A. Coleman, J. E. Bradby, and C. Jagadish, P. Munroe, Y. W. Heo, S. J. Pearton, D. P. Norton, M. Inoue, and M. Yano, Appl. Phys. Lett. **86**, 203105 (2005).
[6] P. Deb, H. Kim, Y. Qin, R. Lahiji, M. Oliver, R. Reifenberger, and T. Sands, Nano Lett. **6**, 2893 (2006).
[7] B. Pérez-García, J. Zúñiga-Pérez, V. Muñoz-Sanjosé, J. Colchero, and E. Palacios-Lidón, Nano Lett. **7**, 1505 (2007).
[8] J. Bauer, F. Fleischer, O. Breitenstein, L. Schubert, P. Werner, U. Gösele, and M. Zacharias, Appl. Phys. Lett. **90**, 012105 (2007).
[9] L. Libioulle, Y. Houbion, and J.-M. Gilles, Rev. Sci. Instrum. **66**, 97 (1995).
[10] S. M. Sze, D. J. Coleman, Jr., and A. Loya, Solid-State Electron. **14**, 1209 (1971).
[11] A. A. Sokol, S. A. French, S. T. Bromley, C. R. A. Catlow, H. J. J. van Dam, and P. Sherwood, Faraday Discuss. **134**, 267 (2007).
[12] C. G. Van de Walle, Phys. Rev. Lett. **85**, 1012 (2000).
[13] M. Grundmann, *The Physics of Semiconductors: An Introduction Including Devices and Nanophysics* (Springer, Berlin, 2006).
[14] F. A. Padovani and R. Stratton, Solid-State Electron. **9**, 695 (1966).
[15] J. Goldberger, D. J. Sirbuly, M. Law, and P. Yang, J. Phys. Chem. B **109**, 9 (2005).
[16] A. Cavallini, L. Polenta, M. Rossi, T. Richter, M. Marso, R. Meijers, R. Calarco, and H. Lüth, Nano Lett. **6**, 1548 (2006).
[17] Y. Lin, D. Wang, Q. Zhao, Z. Li, Y. Ma, and M. Yang, Nanotechnology **17**, 2110 (2006).

Downloaded 23 Oct 2008 to 85.232.23.177. Redistribution subject to AIP license or copyright; see http://jap.aip.org/jap/copyright.jsp